Earth and Planetary Science Letters 442 (2016) 206–217

Contents lists available at ScienceDirect

Earth and Planetary Science Letters

www.elsevier.com/locate/epsl

Rapid thermal rejuvenation of high-crystallinity magma linked to porphyry copper deposit formation; evidence from the Koloula Porphyry Prospect, Solomon Islands

S. Tapster [a,b,*], D.J. Condon [b], J. Naden [c], S.R. Noble [b], M.G. Petterson [a,d], N.M.W. Roberts [b], A.D. Saunders [a], D.J. Smith [a]

[a] Department of Geology, University of Leicester, Leicester, LE17 RH, UK
[b] NERC Isotope Geosciences Laboratory, British Geological Survey, Keyworth, Nottingham, NG12 5GG, UK
[c] British Geological Survey, Keyworth, Nottingham, NG12 5GG, UK
[d] Secretariat of the Pacific Community, Geoscience Division, Fiji

ARTICLE INFO

Article history:
Received 3 August 2015
Received in revised form 4 February 2016
Accepted 24 February 2016
Available online 22 March 2016
Editor: M. Bickle

Keywords:
porphyry copper deposit
zircon
mineralisation
magma
geochronology

ABSTRACT

Magmas containing the components needed to form porphyry copper deposits are relatively common within arcs, yet mineralising events are uncommon within the long-lived magmatic systems that host them. Understanding what causes the transition from barren to productive intrusions is critical to the development of conceptual deposit models. We have constrained the tempo of pre- and syn-mineralisation magmatic events in relationship to the thermal evolution of the plutonic body that underlies one of the world's youngest exposed plutonic–porphyry systems, the Inamumu Zoned Pluton, Koloula Porphyry Prospect, Solomon Islands. High precision ID-TIMS U–Pb dates of texturally and chemically characterised zircons indicate pluton emplacement over <150 kyr was superseded after ca. 50 kyr by two discrete episodes of mineralising porphyritic melt emplacement. Their associated hydrothermal systems initiated within ca. 30 kyrs of each other. Zircon populations within evolved intrusions contain resorbed cores that were recycled from the deeper magmatic system, yet their youngest dates are statistically indistinguishable from those yielded by crystals lacking resorption. Comparisons of Ti-in-zircon proxy temperatures, modelled zircon saturation temperatures and temperature–crystallinity relationships suggest that prior to being heated and emplaced within the shallow level pluton, magmas were stored at depth in a high-crystallinity (>50% crystals) state, past the point of rheological lock-up. We estimate that thermal rejuvenation of the deeper high-crystallinity magma and generation of a mobile melt fraction may have occurred ≤10 kyr before its transport and emplacement within the porphyry environment. The underlying pluton likely cooled and returned to high-crystallinity states prior to subsequent remobilisation-emplacement events. Titanium-in-zircon geothermometry and whole-rock geochemistry suggest pre-mineralisation intrusions were remobilised by mixing of a silicic magma with a high-temperature, less-evolved melt. In contrast, syn-mineralisation melts were most likely remobilised by the percolation of hot volatiles exsolved from contemporaneous less-evolved intrusions cooling beneath the crystalline silicic magma. The evidence for the rapid thermal rejuvenation and long term storage of highly crystalline silicic magmas is consistent with previous studies that indicate two components of exsolved volatiles contribute to ore forming fluids. We conclude that the liberation of crystal-rich porphyry copper deposit forming magmas, and the addition of the chemical components required for ore formation, are intrinsically linked to the volatiles released during the recharge of less-evolved melt into a highly crystalline silicic magma.

1. Introduction

Porphyry copper deposits (PCDs) are fundamental to meeting present and future global demand for metals (Sillitoe, 2010). The precipitation of copper and precious metal ores within single or clustered hydrothermal systems is typically associated with the

* Corresponding author at: NERC Isotope Geosciences Laboratory, British Geological Survey, Keyworth, Nottingham, NG12 5GG, UK.
E-mail address: simont@bgs.ac.uk (S. Tapster).

http://dx.doi.org/10.1016/j.epsl.2016.02.046

intrusion of crystal-rich, porphyritic magmas at shallow crustal levels (1–4 km depth; Sillitoe, 2010). These shallow intrusions act as the "exhaust valve" for larger magmatic systems at depth that are saturated or near-saturated in H_2O. The magmatic systems that underlie PCDs are the source of thermal energy, metals and magmatic volatiles that ultimately form the mineralisation. Empirical observations of PCDs imply a rare set of circumstances within the underlying magmatic systems are required in order to form deposits (Wilkinson, 2013). Understanding the triggers for mineralising magmatic events and how they differ from non-mineralising systems underpins exploration models for finding new deposits.

Traditional models propose that the cooling and crystallisation of a large, convecting, silicic melt body, in addition to depressurisation as mobile magma batches ascend through the crust during intrusion are key triggers for volatile exsolution and PCD formation (Burnham, 1997; Shinohara and Hedenquist, 1997; Sillitoe, 2010). Yet there is a growing body of evidence that silicic plutons typically reside in cool, highly crystalline, immobile states (e.g. Barboni and Schoene, 2014; Cooper and Kent, 2014; Marsh, 1981). Moreover, a critical role for concurrent, more-mafic magmatism in the chemical budget of PCDs has also previously been implied (e.g. Blundy et al., 2015; Halter et al., 2005; Hattori and Keith, 2001). Evidence suggests that volatile components capable of ore formation may not have equilibrated with the silicic magmas they are associated with (Nadeau et al., 2013a), and mafic injection into silicic magma has been implied as a trigger for explosive eruptions and loss of porphyry components to the atmosphere (e.g. Hattori and Keith, 2001; Pasteris, 1996; Wallace and Edmonds, 2011). This raises the question: by what mechanism does mafic magma contribute essential components to the ore forming intrusion?

Large silicic plutonic bodies are built incrementally through numerous recharge events from magmas sourced deeper in the crust (e.g. Leuthold et al., 2012; Menand et al., 2015; Schoene et al., 2012). The style of interaction between silicic plutons and recharging melts is strongly controlled by the thermal-rheological-density properties of the involved magmas (e.g. Couch et al., 2001; Sparks and Marshall, 1986). Likewise, the existence of mobile porphyritic magma, the timing of volatile saturation within both magmatic components, and the ability of volatiles exsolved at depth to be transported through plutonic systems are all strongly controlled by the melt–crystal ratios of the involved magmas (Huber et al., 2010; Lake, 2013; Parmigiani et al., 2014; Shinohara and Hedenquist, 1997).

Constraining the thermal-crystallinity evolution of source magmas with time is therefore essential to our interpretation of PCD formation, yet the difference in emplacement depth between PCDs and their parental plutonic systems makes connected observations within modern and ancient systems problematic. To negate this issue, this study utilises high-precision isotope dilution thermal ionisation mass spectrometry (ID-TIMS) U–Pb geochronology of geochemically (Ti-in-zircon thermometer; Ferry and Watson, 2007) and petrographically characterised zircon populations to constrain residence times and thermal fluctuations in magmas prior to their eruption or emplacement (e.g. Rivera et al., 2013; Schoene et al., 2012). We have applied these techniques to one of Earth's youngest exposed plutonic-PCD systems at the Inamummu Zoned Pluton (IZP), Koloula Porphyry Prospect, Solomon Islands (Fig. 1). The IZP documents an extensive suite of intrusive units that culminated in two discrete magmatic–hydrothermal mineralisation events associated with porphyritic intrusions (Chivas and McDougall, 1978; Chivas and Wilkins, 1977). In this study we examine: the conditions of magma storage preceding PCDs; the duration and triggers of mineralising magmatic–hydrothermal events; and the role of less evolved magmas in generating ore deposits.

2. Geological background

The mineralised IZP forms part of the Plio–Pleistocene Koloula Igneous Complex on the island of Guadalcanal, Solomon Island Arc. Located at the convergent boundary of the Indo-Australian and Pacific Plates, the basalt–rhyolite sequences of the Oligocene–early Miocene Suta Volcanics that host the Koloula Igneous Complex (Fig. 1) were extruded during arc activity related to subduction of

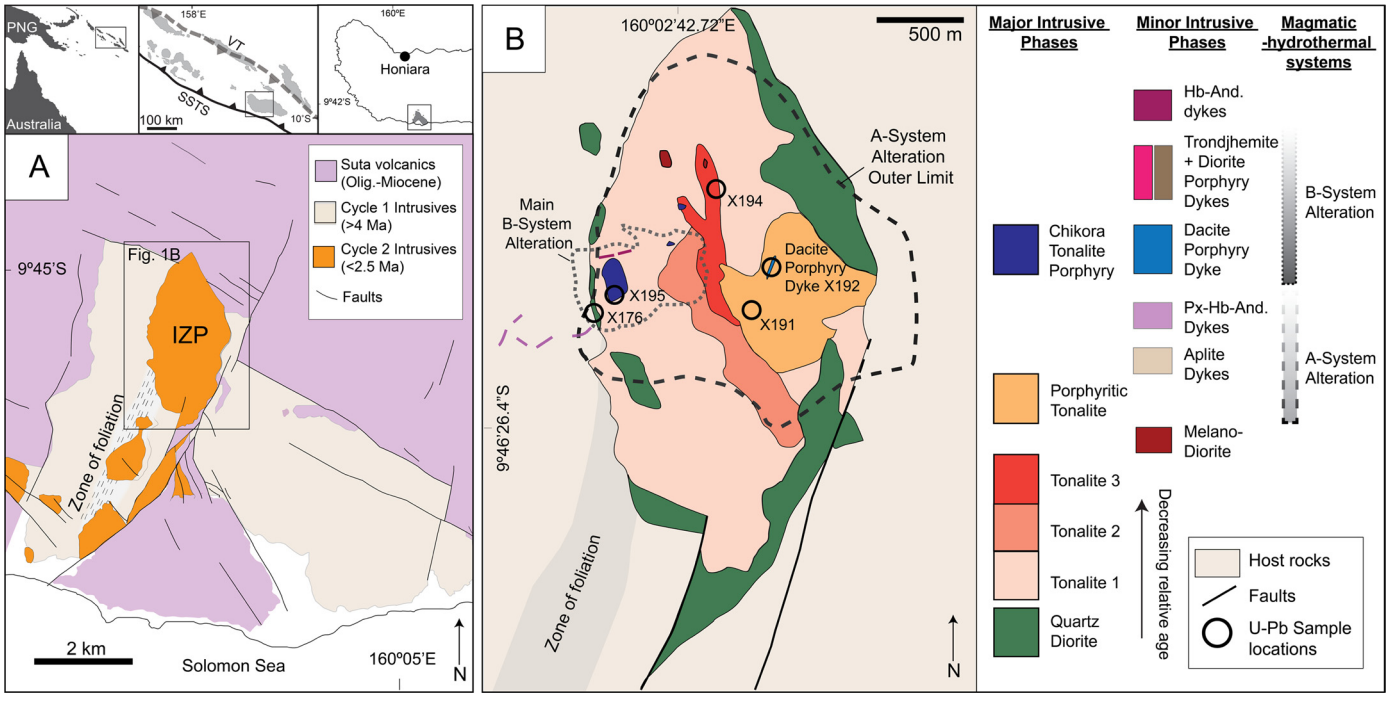

Fig. 1. A) Location map and simplified geological setting of the Koloula Igneous Complex, Guadalcanal, Solomon Island Arc, VT—Vitiaz Trench, SSTS—South Solomon Trench System; B) Simplified lithology map and relative emplacement timings of the of the Inamumu Zoned Pluton after Chivas (1978).

the Pacific plate at the Vitiaz Trench, prior to Miocene subduction zone polarity reversal (Petterson et al., 1999). Following a period of quiescence, arc magmatism was reactivated in the late Miocene–Pliocene due to the subduction of the Solomon Sea oceanic crust at the South Solomon Trench System (Petterson et al., 1999).

In central Guadalcanal, late Miocene–Pleistocene magmatic expressions are confined to an arc-normal lineament that hosts a number of epithermal and porphyry Cu–Au deposits (Chivas, 1978; Swiridiuk, 1998). The Koloula Igneous complex was emplaced over two intrusive cycles, the most voluminous and earliest units were Cycle 1 gabbros–diorites–granodiorites with K–Ar ages of ca. 4–4.5 Ma (Chivas and McDougall, 1978). Cycle 2 intrusions were intruded in close proximity to a 400 m wide foliated zone within the Cycle 1 gabbros, running parallel to the arc-normal lineament. The ~6 km^2 IZP is the most substantial of the Cycle 2 intrusions. Pleistocene-ongoing tilting of the Guadalcanal crustal block has exposed progressively deeper levels towards the South coast (Chivas et al., 1984), with the IZP is now located only ~50 km from the trench, at up to 750 m above sea level.

2.1. Intrusive units and mineralisation of the IZP

The IZP is a concentrically zoned intrusion; the succession of intrusive events (Fig. 1) are described in detail by Chivas (1978), Chivas and McDougall (1978) and outlined below. The earliest igneous units, in contact with the Cycle 1 gabbros, are Quartz Diorites (plagioclase, clinopyroxene, hornblende, biotite, quartz, ±orthopyroxene) that show weakly aligned plagioclase laths (Chivas, 1978). The onset of Quartz Diorite magmatism, inferred at 2.4 Ma by K–Ar dating (Chivas and McDougall, 1978), was followed by Tonalites 1–3, which represent discrete, equigranular tonalite units (plagioclase, quartz, clinopyroxene, biotite, amphibole, K-feldspar) that were sequentially intruded at the centre of the IZP. The tonalite units become progressively coarser grained and show increasing abundances of quartz, biotite and K-feldspar within younger intrusions. Finer grained melanocratic tonalite units cross-cut Tonalite 3 in the north of the IZP.

The Porphyritic Tonalite shares gradational contacts with both Tonalites 3 and 1 where exposed. It contains hornblende, plagioclase, resorbed quartz and biotite phenocrysts (~40% by volume), and quartz ± alkali feldspar filled miarolitic cavities. All earlier major units of the IZP are intruded by aplite dykes and are overprinted by the earliest mineralising magmatic–hydrothermal event, defined as the A-System by Chivas and Wilkins (1977) and Chivas (1978). The A-system contains a zoned alteration envelope from potassic to propylitic assemblages, centred over the Porphyritic Tonalite. Copper sulfides are restricted to hairline fractures. Pyroxene–hornblende andesite dykes were emplaced outside the IZP during the activity of the A-system (Chivas, 1978) and K–Ar dates infer the onset of the A-system and emplacement of earlier intrusive units by ca. 2.1 Ma (Chivas and McDougall, 1978).

A-System alteration is cross-cut by the pipe-like body of the Chikora Tonalite Porphyry, which intrudes Tonalite 1 and, at depth, a breccia pipe that contains clasts of Tonalite 3 and Porphyritic Tonalite (Chivas, 1978). Phenocrysts (~35–50%) consist of: strongly zoned plagioclase, hornblende that is commonly fragmented and engulfed by groundmass, coroded and strained quartz, and minor biotite within an aphanitic groundmass. Miarolitic cavities are infilled with sulfides, indicating the intrusion was synchronous with the B-System hydrothermal event (Chivas, 1978). Recent mineral exploration activity identified a strongly-mineralised, minor, porphyrytic dacite intrusion of equivalent lithology to the Chikora Tonalite Porphyry within the outcrop of the Porphyritic Tonalite (Fig. 1), although no contacts were observed. We refer to this as the "Dacite Porphyry Dyke" herein. The B-system contains semi-pervasive–veined Cu-sulfide and molybdenite mineralisation

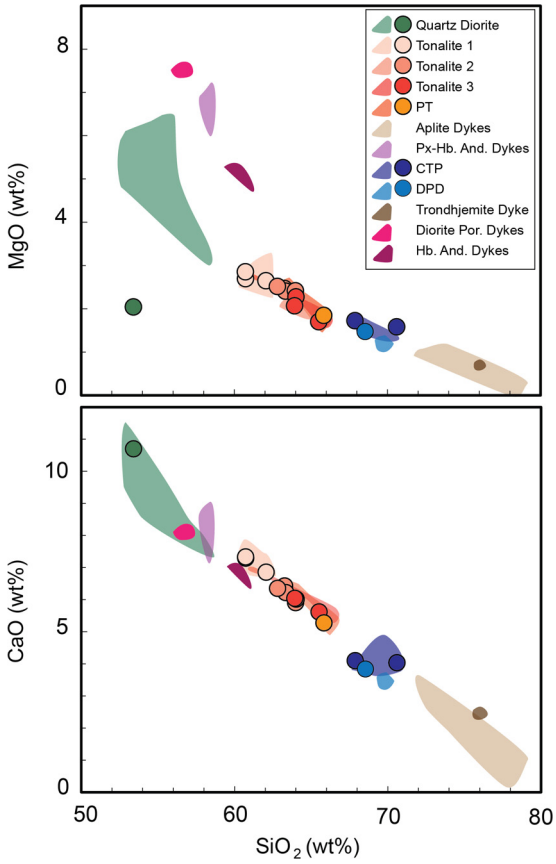

Fig. 2. Major element Harker plots (MgO and CaO) for intrusive phases within the IZP. New data (points) are compared with the whole-rock geochemistry of Chivas (1982) (Shaded fields). Note the linear trend of major intrusive phases (Tonalite 1–3, PT—Porphyritic Tonalite, CTP—Chikora Tonalite Poprhyry, and the DPD—Dacite Porphyry Dyke) and the good comparison between the Chikora Tonalite Porphyry (U–Pb dated sample: X195) and the Dacite Porphyry Dyke (U–Pb dated sample: X192). Major elements are normalised to anhydrous 100 wt% totals.

(Chivas, 1978; Chivas and Wilkins, 1977), with the main potassic to propylitic alteration halo centred over the Chikora Tonalite Porphyry. Drill core has intersected Cu grades of 0.25–0.36 wt% over 152 m (SolGold plc, annual report 2011). Minor trondhjemite and diorite porphyry dykes cross-cut the earliest B-System alteration halo yet contain similar mineralisation-alteration styles and form part of the same B-system event (Chivas, 1978). K–Ar dating infers a 1.7–1.6 Ma emplacement age for the Chikora Tonalite Porphyry, and cooling of the B-system hydrothermal event, likely due to a large influx of meteoric/marine water, by ca. 1.44 Ma, (Chivas and McDougall, 1978; Chivas et al., 1984), when hornblende-andesite dykes were intruded into the B-System alteration envelope (Chivas and McDougall, 1978).

3. Whole-rock geochemistry of the IZP

Sixteen samples from the suite of IZP major intrusions were analysed by X-ray fluorescence at the University of Leicester. Sample details and methods are described within the Supplementary Material (S1 and S2); data are presented within Table A1.

New analyses are in good agreement with the range of compositions defined by Chivas et al. (1982) (Fig. 2; Fig. A3), with the exception of the Quartz Diorite (X176), which has similar SiO_2, but lower total Fe (as Fe_2O_3), MgO, TiO_2 and higher Al_2O_3, CaO and Na_2O, suggesting X176 represents a plagioclase feldspar cumulate. Harker plots (Fig. 2; Fig A3) of the major intrusion suite (Tonalite 1 to Chikora Tonalite Porphyry) define linear arrays, showing decreasing MgO, Fe_2O_3, and CaO with increasing

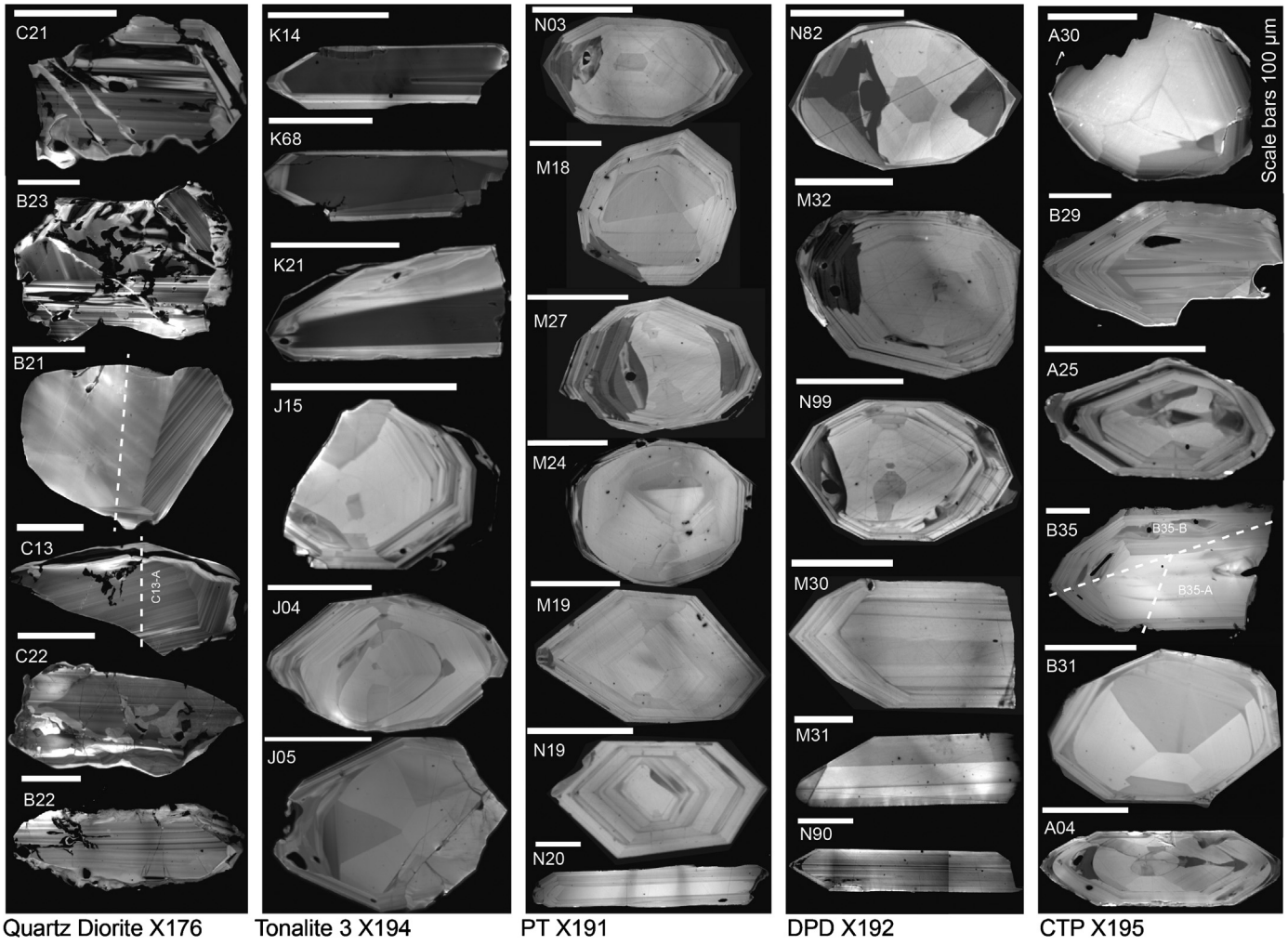

Fig. 3. A) Representative zircon CL images for fractions dated with ID-TIMS U–Pb geochronology. Resorbed, equant sector zoned cores marked by the truncation of zonation are common with the exception of the Quartz Diorite (X176), which contains textures indicative of crystal plastic deformation. Fractions C21 and B23 (X176) were not dated but images are included to demonstrate the extent of these features within zircons from this sample. Scale bars are 100 µm.

SiO_2, and which follow the sequential emplacement relationships within the IZP towards more evolved compositions with time, although with some overlap between Tonalite 3 and the Porphyritic Tonalite. Compositions of the minor diorite porphyry, andesitic, and aplitic dyke phases do not follow the sequential pattern, falling towards more mafic and felsic compositions than the major suite. The Chikora Tonalite Porphyry samples and the Dacite Porphyritic Dyke are closely comparable across all elements.

4. Zircon textures and U–Pb geochronology

Samples from the Quartz Diorite (X176), Tonalite 3 (X194), Porphyritic Tonalite (X191), Chikora Tonalite Porphyry (X195) and the geochemically similar porphyritic dyke (X192) were selected for zircon U–Pb geochronology. Sample details and full analytical protocols are provided in the Supplementary Material (S1 and S2), in addition to further information pertaining to U–Pb data interpretation (S5) presented below. A thermally annealed sub-set of zircons, representative of the sizes and morphologies extracted by heavy mineral separation were imaged by cathodoluminescence (CL) at the University of Leicester, and a further representative sub-set were analysed for trace elements by single collector sector field laser ablation inductively coupled plasma mass spectrometry (SC-SF-LA-ICP-MS) at NERC Isotope Geoscience Laboratories (NIGL). Zircon images with ablation sites and tabulated analyses for Ti, Th, and U concentrations are in the Supplementary Material (S3) and Table A2. A further sub-set of characterised zircons were extracted from epoxy mounts and analysed by chemical abrasion (CA)-ID-TIMS at NIGL augmented by analyses of non-CL imaged zircons ($n = 4$). Isotopic data and dates are presented within Table A3.

CL images (Fig. 3) of the anhedral and inclusion-rich zircons (Fig. A5) extracted from the Quartz Diorite intrusion (X176), show internal structures such as diffuse segments of oscillatory zoning and anastomosing cross-cutting bands, without adjacent displacement or rotation, that indicate crystal plastic deformation of zircon (Kaczmarek et al., 2011; Reddy et al., 2006). Younger, more evolved samples (X194; X191; X195; X192), contain textural populations of: 1) sector-zoned multifaceted equant zircons commonly with resorption surfaces and discordant rim overgrowths with stronger oscillatory zonation; and 2) prismatic, elongate zircons with continuous planar or oscillatory zoning, often around homogeneous cores (Figs. 3 and A6–A9). The Th/U ratios and U concentrations measured by SC-SF-LA-ICP-MS within sector zoned cores and discordant oscillatory zoned rims overlap in their distributions, while analyses from the zircon population without resorption surfaces also overlap, yet range to higher values (Fig. 4). This is most evident in the population of low CL-emission, dark prismatic zircons of Tonalite 3 (X194; Fig. 3), which demonstrate elevated Th/U ratios and U concentrations relative to zircons of younger the porphyritic samples (Fig. 4).

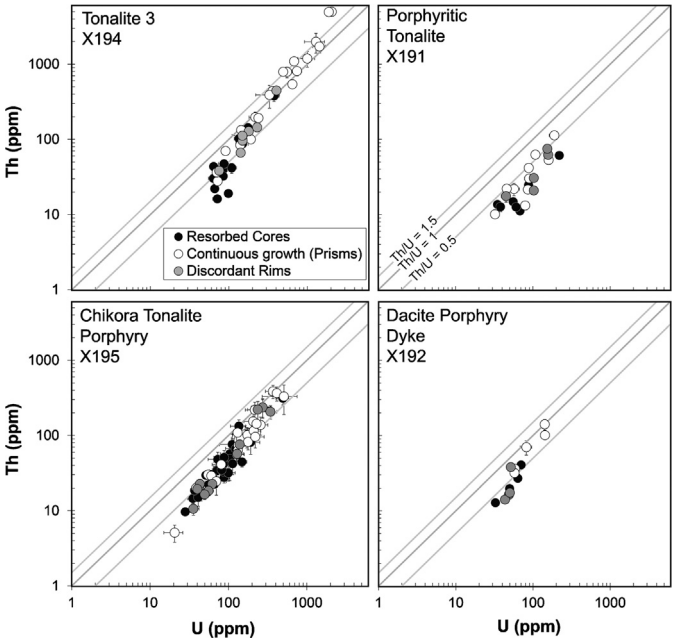

Fig. 4. Uranium and Th concentrations of zircons analysed by laser ablation for different textural populations of the silicic samples analysed by ID-TIMS U–Pb geochronology. Grey lines define Th/U ratios of unity, 1.5 and 0.5.

Two major factors affecting the precision and accuracy of dates arise due to the young nature and typically low U concentrations of the zircons in this study: Firstly, the correction applied for laboratory blank common Pb (Pbc) accounts for the largest component of analytical uncertainty on $^{206}Pb/^{238}U$ dates (Table A2). We excluded data with $^{206}Pb/^{204}Pb < 25$, and used a robust isotopic composition and uncertainty for the laboratory blank Pbc, based upon total procedural blank data over the multi-year period of analysis to give a comprehensive representation of the uncertainty associated with the correction (see Supplementary Material S1). Secondly, varying the assumed magma Th/U used within the correction for initial ^{230}Th disequilibrium within zircon (Schärer, 1984) can significantly alter young $^{206}Pb/^{238}U$. A sensitivity analysis of Th/U_{melt} is provided in the Supplementary Material (S5), it implies that over geologically feasible ranges of Th/U_{melt} the interpretations of emplacement ages and Δ time may vary from those based upon the reported Th corrections at the 10^3–10^4 yr scale. However, reported dates are near maxima and thus our drawn conclusions are unaffected by inaccuracy in the assumed Th/U_{melt}.

Each single fraction analysis is reported with uncertainties in Pbc composition and Th/U_{melt} propagated. These are likely to have some covariance, in which case a component of the Pbc and Th uncertainty should be considered a limiting factor on date uncertainty (Ickert et al., 2015). We report uncertainties on the $^{206}Pb/^{238}U$ dates at the 2σ level, inclusive of tracer calibration and decay constant uncertainties, as the uncertainty budget is dominated by the Pbc correction so that the contributions from systematic sources are insignificant (<1 kyr) and there is no practical need to differentiate these.

Convention in geochronological studies that derive sample age interpretations from multiple dates of single fractions is, typically, to present the weighted means of multiple analyses. Mean square weighted deviates (MSWDs) of weighted means offer statistical control on determining whether scatter between analyses can be resolved outside of that expected from analytical scatter. However, weighted mean dates are predicated with the assumption of uncertainties on a normally distributed, single population. Based upon the textural evidence of zircon presented, the latter is not a valid assumption for all analysed fractions, as resorption surfaces within zircons represent intervals of zircon under-saturation and dissolution at crystal rims prior to a later crystallisation event and discrete stage of melt evolution (Watson, 1996). Alternatively, the 'youngest date', which is often incorrectly confused with the 'youngest zircon', may be interpreted as the emplacement age. However, this has the scientific weakness that it does not require the test of reproducibility to assess analytical scatter, or potential open system behaviour.

Due to the increased confidence from dates being reproduced, our preference for the interpretation of 'emplacement ages' in this study is based upon the weighted mean of the texturally distinct zircon populations without resorbed cores (Fig. 5). However, we are also wary not to substantially reduce uncertainties below the level of the more precise data points and their limiting uncertainties arising from the Th and Pbc corrections by use of the weighted mean algorithm with high-n values. To demonstrate that our choice of interpretation does not influence the derived chronologies, Fig. 6 highlights that different approaches to date selection yield no significant variation.

Six fractions from Quartz Diorite (X176) demonstrating varying extents of sub-solidus alteration yield a weighted mean (Th-corrected) $^{206}Pb/^{238}U$ date of 1.700 ± 0.017 Ma (Figs. 3 and 5). Enhanced diffusion of U, Th and Pb during crystal plastic deformation has the potential to disturb the zircon geochronometer (Reddy et al., 2006). The statistically acceptable MSWD at the 95% confidence interval (CI) suggests that diffusion effects on the U–Th–Pb system are negligible at the level of attained precision. However, the date may be up to ca. 30 kyr younger than that stated if a component of Pbc was contributed to analyses by inclusions (Supplementary Material S5).

For the more evolved samples, 7–12 zircon fractions were analysed by CA-ID-TIMS (Figs. 3 and 5). One fraction with a date of ca. 23.6 Ma (X195) indicates inheritance, likely from the Suta Volcanics. Three dates clustering around ca. 2 Ma (Fig. 5) are attributed to components of xenocrystic zircon recycled from earlier, magmatism within the Koloula Intrusive complex (Cycle 1; Chivas and McDougall, 1978). Weighted mean dates from zircons without resorbed cores yield statistically acceptable MSWDs and our preferred interpreted emplacement ages indicate younging consistent with geological relationships (Fig. 1) from Tonalite 3 to the Chikora Tonalite Porphyry and Dacite Porphyry Dyke over ca. 1.55–1.46 Ma (Figs. 5 and 6). The MSWDs of weighted means yielded by all analysed fractions within porphyritic samples (X191; X192; X195) indicate resolvable geological scatter. As highlighted by their probability density distributions (Fig. 6), fractions with resorbed cores range to older dates than interpreted emplacement ages of the previous intrusion(s).

Within X194, X191 and X192, weighted means for the clusters of youngest dates yielding statistically acceptable MSWDs from the resorbed core textural populations are similar to the dates of the textural population without resorbed cores (Fig. 6). As textural evidence dictates these do not represent the crystallisation of a single population, rather a mixture of core and rim crystallisation episodes, their dates must represent the maximum possible age for the crystallisation of the emplaced magma, further demonstrating that dates conform to intrusive relationships. Resorbed cores of the Chikora Tonalite Porphyry (X195) form a weighted mean date older than the preferred emplacement age and between the dates of X191 and X194. However, the youngest date of a fraction with a resorbed core is comparable to those without cores, similar to the other porphyritic samples.

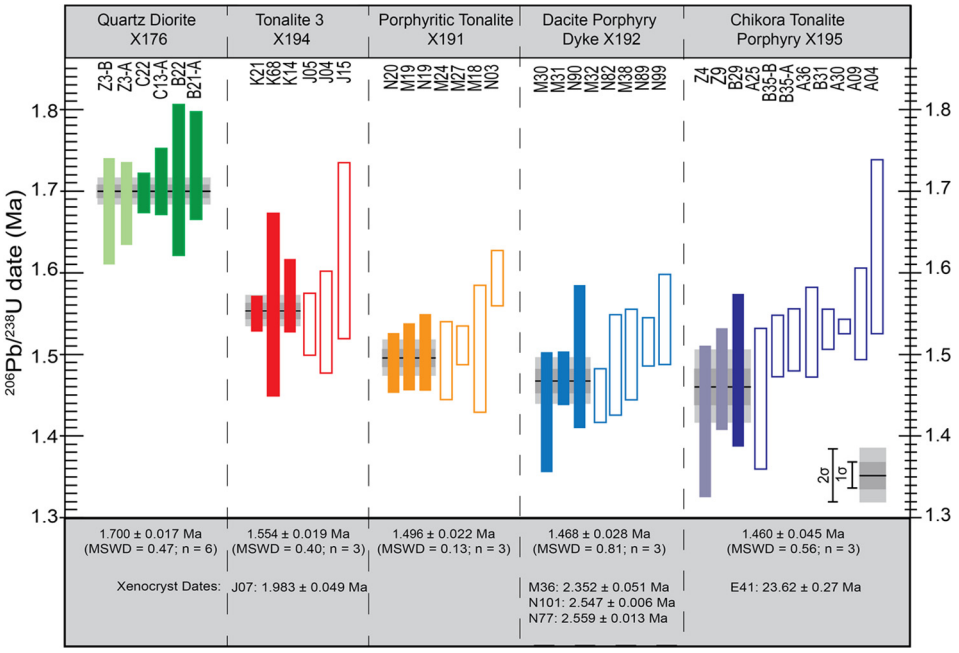

Fig. 5. ^{230}Th disequilibrium corrected ^{206}Pb/^{238}U dates and weighted mean dates taken as preferred emplacement ages from textural populations without resorbed cores. Boxes represent 2σ uncertainty for single fractions. White boxes with coloured outlines—fractions with resorbed cores; Fully shaded boxes—fractions without resorbed cores; Pale coloured boxes—denotes fractions that were not CL imaged, in the case of X195 the two fractions have an elongate-prismatic morphologies consistent with zircons without resorbed cores (Figs. A6–A9). Single fraction dates of zircons older than the Quartz Diorite are interpreted as xenocrysts and listed in grey boxes below their respective samples. See text for further discussion. (For interpretation of the references to color in this figure legend, the reader is referred to the web version of this article.)

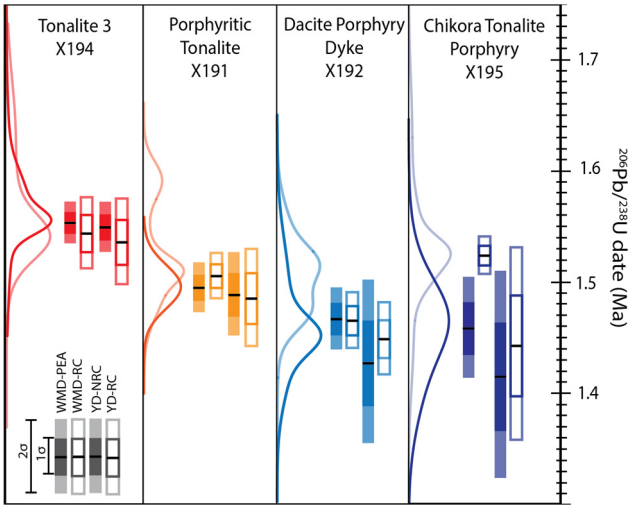

Fig. 6. Comparisons of ^{206}Pb/^{238}U (^{230}Th corrected) date interpretations and probability density distributions (pale lines—dates from fractions with resorbed cores; darker lines—dates from prisms with continuous growth) for the two textural populations. WMD-PEA—Weighted mean date of the preferred emplacement age taken from the textural population without resorbed cores; WMD-RC—Weighted mean date of the youngest cluster of dates from fractions with resorbed cores that form an MSWD acceptable at the 95% CI; YD-NRC—Youngest date of a fraction without a resorbed core; YD-RC—Youngest date of a fraction with a resorbed core. See text for further discussion.

5. Ti-in-zircon thermometry

Titanium concentrations within zircons younger than the Quartz Diorite show distinct distributions according to textural populations and intrusive unit. Fig. 7 demonstrates that the sector-zoned resorbed cores show narrow distributions of Ti concentrations (4–14 ppm) with major peaks at 5–10 ppm within all samples. Core Ti concentrations are similar to those of discordant rim overgrowths within X191, X192 and X195, and show peaks in probability density functions that overlap with those of zircons without resorption surfaces. The dark prismatic zircons without resorbed cores of Tonalite 3 (X194), demonstrate a much greater range of Ti concentrations with a dominant peak ~16 ppm, and a shoulder ~8 ppm that corresponds to the dominant peak of Ti concentrations within the resorbed cores. The Ti concentrations of X194 discordant rims span the range between resorbed cores and dark prismatic populations.

The empirically derived correlation between temperature of crystallisation and Ti concentration within zircon can be used as a geothermometer within a given model of magma Ti and Si activities (Ferry and Watson, 2007). Greater Ti concentrations within zircon correspond to higher temperatures of crystallisation. As the mineralogy of studied samples contains abundant quartz and titanite, we have assumed a Si activity at unity and a Ti activity of 0.7 (Hayden and Watson, 2007). Within these parameters, Ti concentrations between 5–10 ppm correspond to temperatures of between 715–780 °C, whereas 16 ppm corresponds to a temperature of 830 °C (Fig. 7). The selection of Ti activity at 0.7 makes these maximum temperatures, as the presence of titanite indicates the minimum Ti activity. Varying Ti activity by ±0.1 varies the mean temperature of all analyses by +13.0 °C (1σ = 1.2 °C) and −15.4 °C (1σ = 1.4 °C). Distributions are skewed towards higher temperatures by the absence of analyses that were below detection limits. Further details of thermometry parameters are presented in the Supplementary Material (S4).

6. Discussion

6.1. Tempo of IZP emplacement and mineralisation events

The emplacement of the marginal Quartz Diorite (X176) no earlier than ca. 1.7 Ma in contact with the foliated early gabbro unit decreases the age of the onset of magmatism within the IZP by >700 kyr relative to the K–Ar age of Chivas and McDougall (1978). Crystal plastic deformation of zircon, as evident within the

Quartz Diorite, is commonly associated with tectonically-induced zones of high strain within the crust (Kaczmarek et al., 2011; Reddy et al., 2006). In combination with faults (parallel to the NNE–SSW foliation zone) that cross-cut Tonalite 1 (Fig. 1), and weakly aligned plagioclase laths within the Quartz Diorite (Chivas, 1978), these features indicate a syn-deformation initiation of magmatism within the IZP, likely in a transtensional regime.

The <150 kyr emplacement duration of the equigranular intrusive phases (Quartz Diorite–Tonalite 3), which compose the majority of the IZP, is comparable to the $\sim 10^5$ yr emplacement durations of similarly sized, shallow crust, incrementally-assembled plutons (e.g. Leuthold et al., 2012; Schoene et al., 2012). A minimum 58 ± 29 kyr period of relative magmatic quiescence within the IZP is defined between the non-mineralising Tonalite 3 (X194) and the onset of the A-system magmatic–hydrothermal mineralisation, hosted by, and centred upon the Porphyritic Tonalite (X191) (Chivas and Wilkins, 1977; Chivas, 1978). The main B-system alteration envelope is centred upon the Chikora Tonalite Porphyry (X195), which hosts sulfide in-filled miarolitic cavities (Chivas, 1978) and shares similar geochemistry, mineralisation and dates with the Dacite Porphyritic Dyke (X192). We suggest these intrusions were the expression of the same magmatic event at ca. 1.46 Ma that initiated the B-system hydrothermal activity. Owing to cross-cutting relationships the duration of the A-system mineralising event can therefore constrained by a period of 28 ± 36 kyr, followed in rapid succession by an additional, discrete magmatic–hydrothermal system associated with geochemically distinct intrusions. Our results support the notion that composite mineralisation events within PCDs form at the <100 kyr timescale (von Quadt et al., 2011), and do not preclude that single mineralisation events can form on <10 kyr timescales.

6.2. Evidence for protracted zircon growth and rapid recycling

The silicic intrusions of the IZP demonstrate ubiquitous textural evidence of multi-stage episodic zircon growth, such as resorption surfaces, and changes in the style of zonation from core to discordant rim domains. Textural evidence for protracted crystallisation of zircons preceding intrusion into the IZP is supported by spreads in single fraction dates that lie outside the statistically acceptable limits of analytical scatter at the hand sample-scale of their host unit, a common feature of incrementally assembled plutons (e.g. Schoene et al., 2012).

We interpret the U–Pb dates of the zircons with resorbed cores and younger than ca. 1.7 Ma as containing a component of antecrystic zircon: zircon crystallised earlier within the same magmatic system, yet not within their host intrusion (Miller et al., 2007). When interpreting single fraction U–Pb dates it must be considered that they represent the averaged date of the growth history, and are weighted according to the volume and U concentration of the mixing components. Zircons with resorbed cores within the young porphyritic samples (X191; X192; X195) yield a statistically significant spread of dates (at the 95% CI) that overlap with, or are older than, the emplacement ages of earlier intrusive units. This requires the resorbed cores to contain a growth component older than the preceding IZP intrusion. It is therefore reasonable that the range in dates supports that zircons, and by extension the mobile batches of porphyritic magma that transported them to the IZP, were periodically recycled from a common parental magma source beneath the IZP.

Zircons with resorbed cores also yield dates statistically indistinguishable from the interpreted emplacement ages of their host intrusion and significantly younger than the interpreted emplacement ages of previous intrusions (Figs. 5 and 6). Cores and discordant rim domains typically overlap over narrow ranges of U concentrations (Fig. 4), thus the averaged fraction date is unlikely to be heavily biased towards growth following resorption due to U concentration alone, although the discordant rim population is skewed towards higher U concentrations within Tonalite 3. Discordant rim growth also likely represents the lesser volumetric fraction. CL images suggest approximate core to rim ratios within the young clusters of up to 9:1 (Figs. 3 and 5). With these criteria our calculations suggest a date 40 kyr older than its respective emplacement age will be yielded by a core that predates rim formation by ~55 kyr (Supplementary Material S5).

However, the antecrystic cores also contain mixtures of older and younger crystal growth themselves. Zircon growth and dissolution rates vary according to the melt temperature, the degree of zircon saturation, and are inversely proportional to radial lengths (Watson, 1996), leading to the potential of resorbed cores to yield mean dates significantly older than their youngest crystal growth. Furthermore, the mean dates of cores have been biased towards their older components when their youngest crystal growth was erased due to resorption. Due to the inversely proportional relationship of radius and growth rate, even small degrees of resorption can have significant apparent ageing effects on the date yielded by the entire fraction.

We suggest that to produce the array of dates (Figs. 5 and 6), at least some resorbed sector zoned cores must have been crystallising much less than ~55 kyr before being resorbed and recycled into their respective intrusions within the IZP, and that zircons recycled from depth into the young porphyritic intrusions as resorbed cores were crystallising after the intrusion of Tonalite 3. Likewise, it is probable that the antecrystic cores recycled by the intrusions that generated the B-system mineralisation contain (or contained) crystal growth that occurred after Porphyritic Tonalite emplacement.

6.3. Conditions of magma storage

There are several indicators of the environment in which antecrystic zircons evolved prior to recycling into the IZP intrusions. Equant morphologies and low aspect ratios in zircon are indicative of slow cooling rates or low zircon supersaturation (Corfu, 2003; Vavra, 1990). Sector zonation within zircon has been associated with slow crystal growth and low diffusivity within the reservoir from which a zircon crystallises (e.g. Watson and Liang, 1995). In contrast, pyramid growth and elongation results from greater super-saturation (Vavra, 1990), and oscillatory zonation results from dynamic conditions at the melt–crystal interface, which may reflect convective stirring of the magma (Hoskin, 2000). The Ti-in-zircon thermometry (Fig. 7) demonstrates that the resorbed sector-zoned zircon populations consistently overlap with the peaks within the prismatic crystals and discordant rim domains. The latter can be reasoned to be an approximation for the zircon crystallisation temperatures upon magma emplacement and cooling within the IZP. Temperatures of zircon crystallisation during magma storage, if not crystallisation rates, were therefore comparable to crystallisation temperatures following final emplacement.

Taking into account the temporal distribution of zircons with resorbed cores, the thermometry points towards magma within the common reservoir beneath the IZP being stored for extended periods in a low temperature, near-solidus, high-crystallinity state. This could explain the textural styles observed in zircon cores as: firstly, the latent heat of crystallisation and decreasing thermal gradients to the country rock sustain low-temperature conditions and reduce cooling rates within magmas (Huber et al., 2010; Marsh, 1981); and secondly, interlocking crystals limit magma mobility at >40% crystallinity, and render magmas as rigid bodies unable to convect at >50% crystallinity—retarding heat-loss and lim-

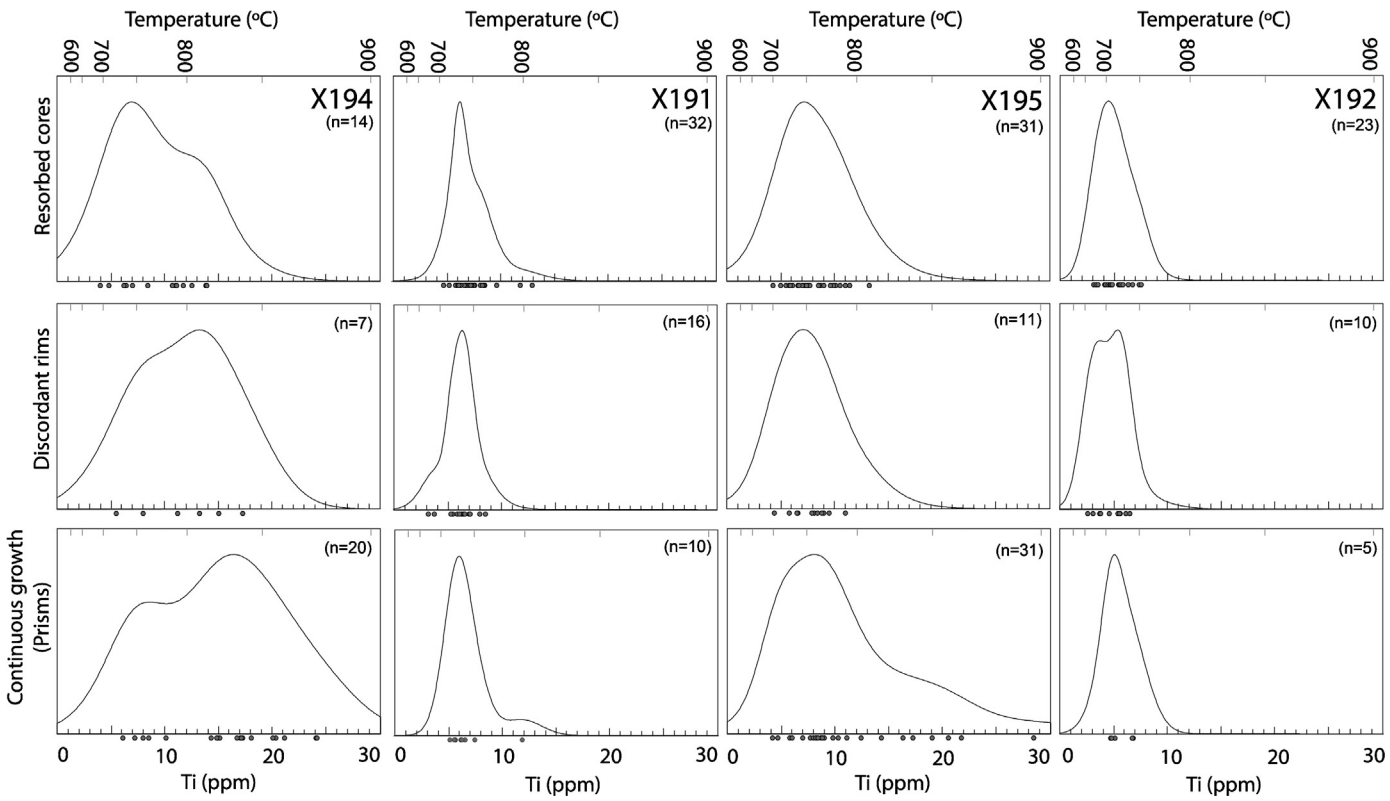

Fig. 7. Titanium concentrations (with 2σ uncertainties) and corresponding Ti-in-zircon temperatures probability density distributions for zircon textural populations and the domain of the ablation site. Grey points indicate single analysis values.

iting melt extraction to crystal-poor interstitial liquid (Bachmann and Bergantz, 2004, 2006; Huber et al., 2010).

To further test this hypothesis we used the Rhyolite-MELTS package (R-Melts; Gualda et al., 2012) to model magma crystallisation and zircon saturation temperatures (Boehnke et al., 2013) in the hypothetical parental magma source beneath the IZP. Models were run over a range of geologically reasonable temperatures (1000–700 °C), pressures (1–3 kbar) and magmatic H_2O (2–6 wt%). Whole-rock geochemistry of the IZP defines a linear array that indicates mixing between mafic-intermediate and silicic components (Fig. 2). Thus we assume the composition of the evolved parental magma prior to porphyry events can be approximated by a composition between Tonalite 3 and the Dacite Porphyry Dyke (see Supplementary Material S6 and Table A4).

Comparisons between crystallinity–temperature relationships and Ti-in-zircon temperature distributions (Fig. 8) support that the antecrystic sector-zoned, resorbed cores crystallised within magma dominantly above the mobility threshold of 50% crystals. Model runs with 4–6 wt% initial H_2O are either initially saturated in volatiles or begin exsolving H_2O at 880–765 °C (Table A4). For simplicity, we assumed that exsolved volatiles were not degassed or segregated, and acted as a fluid component within the three phase (crystal–bubble–melt) magma volume (Pistone et al., 2013). However, as demonstrated in Fig. 8, in the likely eventuality of volatile-loss occurring, magma crystallinities would at a given temperature by both reducing the effective bulk H_2O of the magma, and increasing the relative proportion of crystals within the three phase system.

Zircon saturation temperatures (Fig. 8), are both consistent with the Ti-in-zircon crystallisation temperatures for the resorbed sector-zoned populations and, even under the conservative model parameters employed (Supplementary Material S6), demonstrate that zircon saturation within the melt is driven principally by extensive crystallisation (<50% melt by volume) of the major mineral phases, in which Zr behaves incompatibility. This relationship indicates that zircon growth, and preservation of its chronological record, is only initiated after the magma temperature reduces below the narrow interval over which rapid crystallisation and rheological lock-up occurs (Fig. 8), and when magmas reside in a volatile saturated state (Supplementary Table A4).

In summary, zircon textures and thermometry indicate that the magmas which fed the silicic intrusions of the IZP were stored in a highly crystalline state that rendered the parental magma body immobile for significant episodes between intrusive events within the IZP. Both direct evidence (Barboni and Schoene, 2014) and numerical modelling (Shinohara and Hedenquist, 1997; Spera, 1980) of pluton crystallisation timescales demonstrate that single volumes of hydrous magma, capable of supplying the entire volatile mass budgets for PCD formation (e.g. 50 km^3; Shinohara and Hedenquist, 1997) will reasonably crystallise past the point of rheological lock-up within 1–10 kyr timescales. The orders of magnitude of these timescales are therefore consistent with the pluton underlying the IZP residing as a high-crystallinity magma in the periods between the pulsed IZP melt emplacement events.

6.4. Thermal rejuvenation and remobilisation of magmas

Given that the magma body beneath the IZP spent prolonged episodes in an immobile state, it follows that additional heat was required to remobilise the melts that formed the IZP. Empirical evidence of periodic increases in magma temperature, and a resultant transfer of the magma to a zircon undersaturated state, is provided by the resorption surfaces within antecrystic zircon (Watson, 1996). Zircon saturation temperatures (Fig. 8) indicate the temperatures at the onset of zircon resorption and the liberation of crystal-rich mobile melts (<50% crystals) were closely comparable within the underlying pluton. Therefore, the residence times of zircon cores within zircon undersaturated melt act as proxies for the

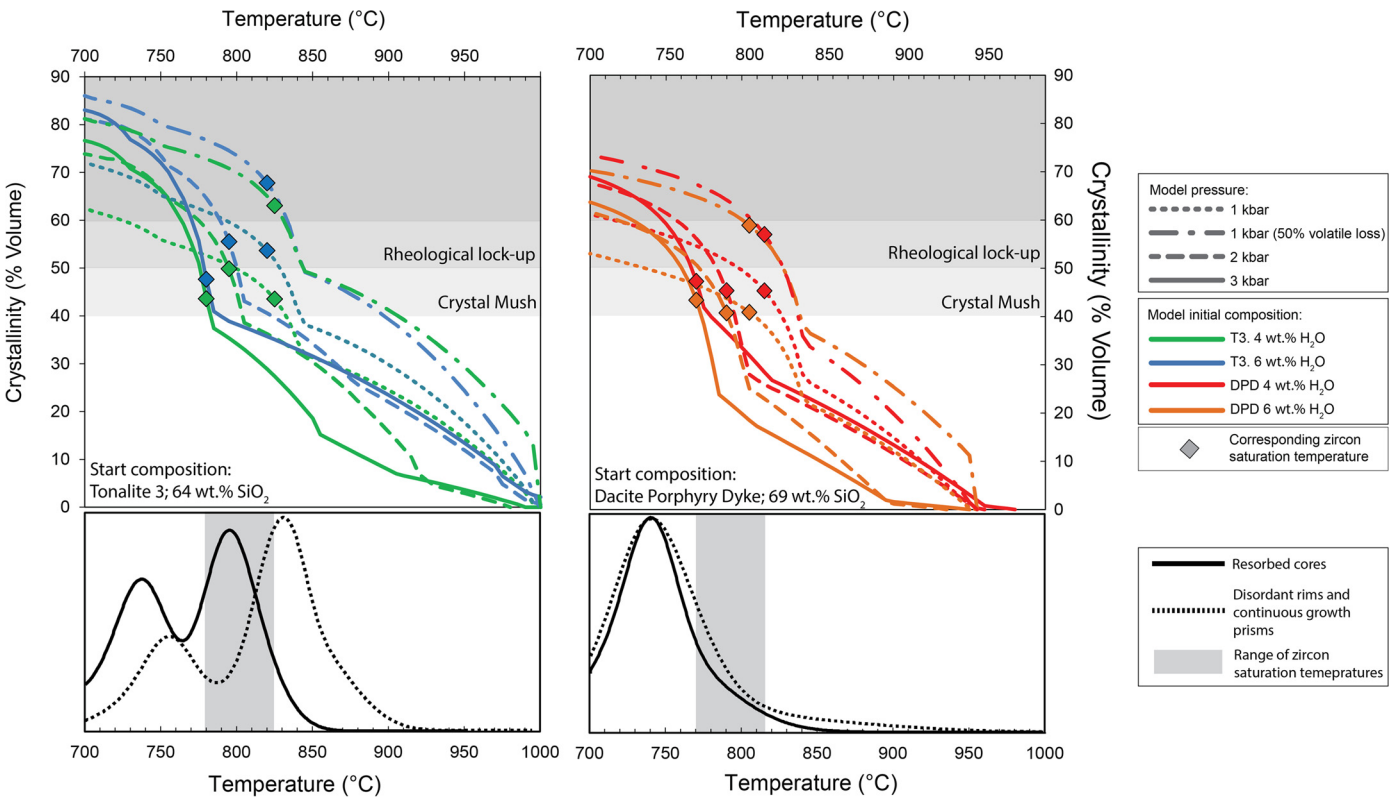

Fig. 8. Rhyolite Melts model Crystallinity–temperature plots for start compositions of A) Tonalite 3 and B) The more silicic Dacite Porphyry Dyke (comparable to the Chikora Tonalite Porphyry), which we assume to represent possible end-member compositions of the silicic pluton underlying the IZP from which these magmas were sourced. Model runs were conducted at 1, 2 and 3 kbar with 4 and 6 wt% initial H_2O. The effects of 50% degassing or volatile segregation from the magma volume are presented for runs at 1 kbar to highlight both the large increase in relative crystallinity that loss of these volatiles would generate and the high % volumes occupied by permeability forming volatiles within the magma. Model runs with 2 wt% H_2O (Supplementary Table A4) have significantly higher crystallinities at a given temperature than runs with greater initial H_2O. Calculated zircon saturation temperatures are depicted with diamonds for their corresponding model run. Crystallinity–temperature relationships are compared with Kernel Density Plots (Vermeesch, 2012) of Ti-in-zircon crystallisation temperatures (lower panels) for the textural populations from (A) non-mineralising equigranular Tonalite 3 (X194) and (B) the cumulative distributions of porphyritic intrusions associated with mineralisation (X191, X192, X195). As noted in Section 5 Ti-in-zircon temperatures are maximums owing to the use of a minimum Ti activity. See text for further discussion.

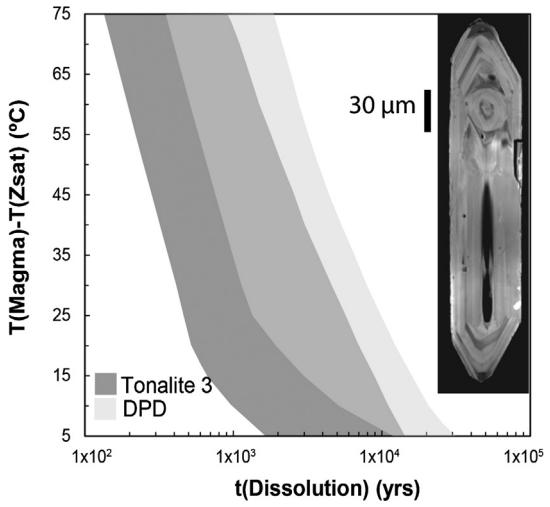

Fig. 9. Dissolution times for a zircon with a 20 µm radius at a constant temperature above the zircon saturation temperature and corresponding zircon undersaturation in the R-Melts model runs at 1–3 kbar and 4 or 6 wt% H_2O. Data is shown as different fields for the two different start compositions, with mid-grey denoting overlap between the model results. See text for discussion. Inset zircon CL image shows a resorbed core of 15 µm radius within zircon A26 of X195 (Chikora Tonalite Porphyry).

durations of the existence of mobile magmas. Resorbed cores with a minimum 15 µm radius were identified within CL imaged grains (Figs. 9 and A6–A9). Conservatively assuming a zircon core radius of 20 µm and using the spherical zircon dissolution rate equations of Watson (1996) where Zr undersaturation is calculated from the R-Melts models (Supplementary Material S6 and Table A4), the maximum residence time within a melt at 5 °C above its saturation temperature can be estimated as 3–30 kyrs (Fig. 9). If the magma temperature increased by a further 15 °C then complete dissolution would occur in 0.6–12 kyrs. These approximations for the brief durations of magma remobilisation-emplacement within the IZP are consistent with the source pluton typically residing in a high-crystallinity state between remobilisation events.

The dominant temperature peak of zircons without resorbed cores in Tonalite 3 is ~50 °C higher than those with (Figs. 7 and 8), and it exceeds Tonalite 3 zircon saturation temperatures (Fig. 8). This suggests their crystallisation initiated within a hotter magma of different composition to the final intrusion. Similar contrasting Ti-in-zircon temperatures are found within other mineralised igneous complexes between andesitic intrusions and lower temperatures derived from evolved intrusions (Dilles et al., 2015). The Th/U of the high-temperature prismatic zircon population are also significantly higher than the sector zoned cores (Fig. 4), also a feature consistent with zircon crystallisation within hotter and less evolved magma compositions (e.g. Harrison et al., 2007; Kirkland et al., 2015). Thus, Tonalite 3 was generated following the intrusion of a high-temperature, less evolved melt, into high-crystallinity magma. It follows that for the high temperature zircon cargo to occur at the hand-sample scale within Tonalite 3, significant mass transfer due to extensive hybridisation must have occurred, consistent with the linear arrays within whole-rock chem-

istry Harker space (Fig. 2). In turn, mixing of magmas requires that the thermal equilibrium reached upon their interaction was above both their crystal lock-up temperatures (Sparks and Marshall, 1986).

Within younger porphyritic intrusions, antecrystic resorbed cores, discordant rims, and prismatic zircons associated with mineralisation all have similar temperatures peaks (Figs. 7 and 8). The thermal rejuvenation events that generated the mobile magmas of the younger porphyries, without the extensive addition of high-temperature zircons, occurred by a different process to that of Tonalite 3. The intrusion of andesitic dykes close to the IZP during the A-system hydrothermal event, and similarly less-evolved dykes late in, and after, the B-system around the Chikora Tonalite Porphyry (Fig. 1; Chivas, 1978) implies that magma recharge remained andesitic, yet imparted thermal energy to the silicic magma with limited mass transfer, by percolating hot volatiles through it.

In the case of andesite recharge to a highly crystalline silicic magma, the contrasts in the density and rheology of magmas cause the andesite to spread beneath the silicic mush barrier (Couch et al., 2001), preventing mixing and chemical equilibration. Where sufficient thermal disequilibrium exists, the recharging andesite will cool towards the lower temperature of silicic magma, causing it to crystallise and saturate in volatiles, if not already having begun degassing during its crustal ascent to the silicic pluton. Heat transport to the overlying silicic magma will predominantly be through the percolation of these exsolved volatiles; diffusion and conduction at the magmas' interface make up only minor components of heat transfer (Bachmann and Bergantz, 2006; Huber et al., 2010). Amphibole within the andesite dykes (Chivas, 1978) requires that they contained 3.5–4 wt% H_2O (e.g. Richards, 2011) and plausibly met the >4 wt% H_2O threshold required to efficiently remobilise overlying silicic crystal mushes though the transfer of heat by exsolved volatiles (Huber et al., 2010).

6.5. The role of magma dynamics in PCD formation

Traditional models of porphyry copper formation, in which large, single melt batches exsolve volatiles upon cooling and/or decompression (e.g. Candela and Holland, 1986; Shinohara and Hedenquist, 1997), are inconsistent with our data set that demonstrates that PCDs in the IZP followed the transient thermal perturbation of a large, high-crystallinity pluton generated during the first ca. 150 kyr of magmatic activity. Rheologically locked, low temperature magma storage has major implications for models of PCD genesis. Firstly, the silicic pluton will become extensively saturated in volatiles over extended (10^4 yr) periods before the emplacement of shallow porphyritic melts. Given the temporal relationships, and as suggested by Blundy et al. (2015), it is unlikely that this volatile component is the main ore-forming fluid. Rather, it is open to the concept of residual brine accumulated within the silicic magma at depth, while SO_2 may be lost within a vapour phase by fumarolic activity (Blundy et al., 2015; Nadeau et al., 2013b).

A number of studies propose that S ± metals crucial for PCD formation are added by volatiles exsolved from less-evolved magmas intruded beneath the silicic plutons (Blundy et al., 2015; Halter et al., 2005; Hattori and Keith, 2001; Nadeau et al., 2013a, 2013b; Zajacz and Halter, 2009). Fig. 10 outlines the possible scenarios during recharge events. In the case of thermal equilibrium between silicic and andesitic–basaltic magmas occurring above their rigid threshold temperatures, requiring high- or sustained heat flux to the silicic pluton, extensive mixing occurs. Sulphur will be sequestered as sulfides and/or anhydrite within the hybrid plutonic magma, and partitioned into fluids that are readily released to the atmosphere upon ascent of the high-temperature, high-volume magma (Nadeau et al., 2013b; Wallace and Edmonds, 2011). If volatiles released from deeper degassing basalts–andesites are injected into the base of a silicic magma with high melt fractions (>50–60%), or low volatile contents (<4 wt% H_2O), the upwards migration of volatiles will be inhibited (Huber et al., 2010; Parmigiani et al., 2014). The silicic magma will be insulated from chemical-thermal inputs at the recharge interface, leading to a stalled and isolated horizon of volatile-enriched and likely hybrid melt.

In contrast, high-crystallinity silicic magma will contain a rigid crystal network with a high-permeability resulting from extensive volatile saturation. These act as conduits for the efficient upwards percolation of S ± metals within, or attached to (Mungall et al., 2015), volatiles released from a recharging, more mafic, magma ahead of the re-melting zone (Huber et al., 2010; Parmigiani et al., 2014; Wallace and Edmonds, 2011), as well as enhancing metal extraction from the remaining silicic melt (Huber et al., 2012). The reaction of accumulated (Cl-rich, S-poor), and injected (S-rich) volatile components may produce the ore forming hydrothermal fluids (Blundy et al., 2015). In addition to imparting chemical components, the addition and percolation of hot volatiles through existing permeable networks in high-crystallinity silicic magma is an efficient means of distributing heat and generating a mobile melt fraction (Bachmann and Bergantz, 2006; Huber et al., 2010; Parmigiani et al., 2014). Increasing the volumetric proportion of bubbles will also reduce the magma viscosity (Pistone et al., 2013).

We suggest that the upwards percolation of hot, S ± metal bearing volatiles released from underlying, less-evolved magma is therefore intrinsically linked to the thermal rejuvenation of the high-crystallinity silicic magma, allowing the magmatic transport of ore forming components to the PCD environment within crystal-rich porphyritic melts. Zircon resorption may have been a fortuitous occurrence of saturation temperatures that lie near the mobile-rigid threshold transition in the studied example. However, rapid thermal fluctuations in the parental magma are likely to be present as dissolution surfaces and overgrowths in the lower-temperature major mineral phases of the source pluton's remobilised crystal residues, present as phenocryst phases within the porphyritic melts associated with ore formation. Internal resorption surfaces within quartz phenocrysts or embayed "quartz-eyes" are one such feature of the mineralising intrusions of the IZP magmas (Chivas, 1978) and are commonly found as phenocryst components within PCDs (Harris et al., 2004; Vasyukova et al., 2013). Their diverse internal growth-resorption textures (Vasyukova et al., 2013) may be indicative of thermally rejuvenated high-crystallinity magmas at depth, in addition to potential resorption during rapid adiabatic ascent upon liberation of mobile melt batches.

Large PCDs form due to the accumulation of numerous discrete magmatic-mineralisation events, which are temporally clustered within the lifetimes of long-lived systems (Sillitoe, 2010). The pluton underlying the IZP was likely limited to only two major cycles of cooling and thermal rejuvenation that favoured mineralisation. These followed the emplacement of Tonalite 3 and were before the system's apparent thermo-rheological death after which the late andesitic dykes intruded. The thermal conditions that govern the fate of magma interaction upon source pluton recharge (i.e. hybridisation, volatile injection, or cross-cutting intrusions), are ultimately controlled by the rate at which heat is supplied to the pluton, relative to heat-loss (Pistone et al., 2013). Consequently the rate of magma flux from deeper in the crust, which will vary over the durations of long-lived magmatic systems, can control the timing and duration at which optimal conditions for PCD formation occur.

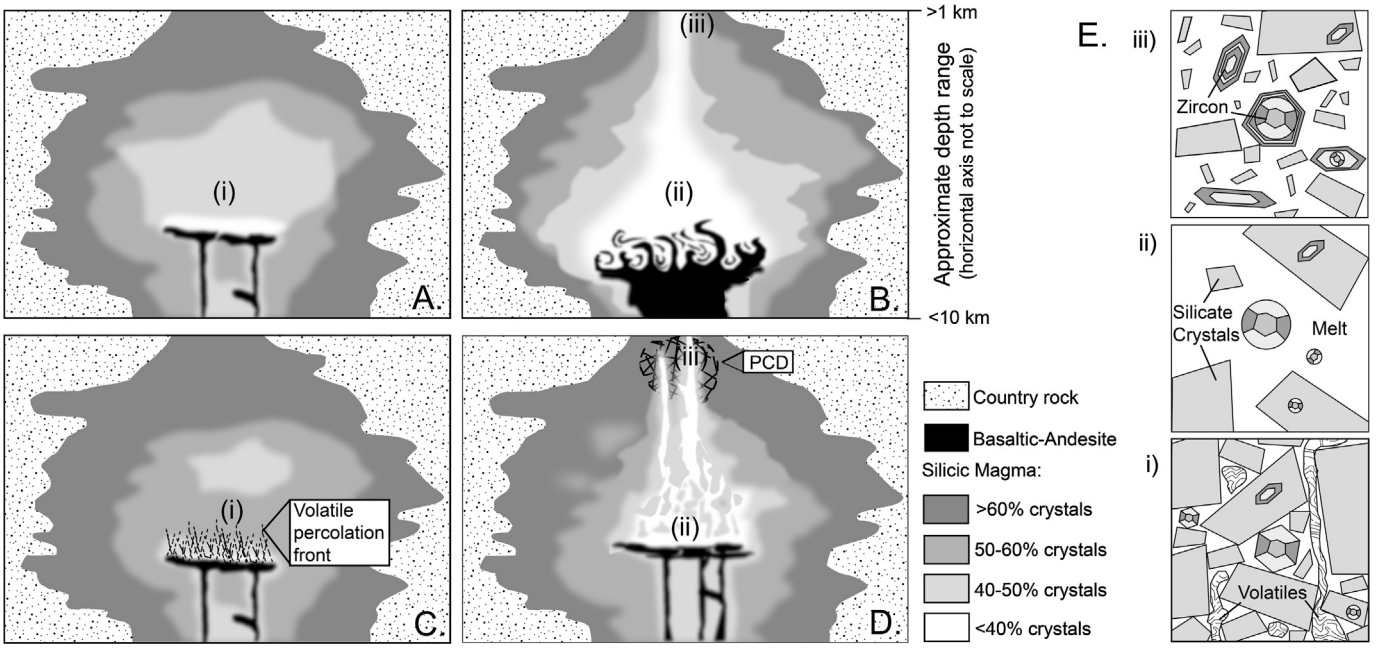

Fig. 10. Conceptual model for different styles of interaction between intruding basaltic–andesite magma and the existing silicic pluton at various states of magma crystallinity during the evolution of the overlying IZP, and corresponding evolution of the observed zircon textures. A) Low flux of recharging magma interacts with a pluton with <50% crystals. Contrasts in the density and rheology prohibit mixing and insulate the silicic pluton from volatiles exsolved from the recharging magma leading to a narrow, volatile-enriched, melt zone at the interface that is likely to be hybridized; B) Continuing recharge or high magma fluxes from depth allow thermal equilibrium at higher temperatures allowing extensive mixing and sequestration of S within minerals or sulfide melt dispersed throughout the pluton. We suggest this represents the type of interaction leading to the remobilisation and emplacement of Tonalite 3 magma; Panels C to D show the progressive remobilisation of a pluton at >50% crystals. Low melt to crystal + volatile ratios within the silicic pluton allows for the percolation of hot S-rich exsolved volatiles into the overlying magma chamber upon magma recharge, with the volatile percolation front advancing ahead of the melting front (Huber et al., 2010). The injection of hot S-rich volatiles into the Cl-rich fluids accumulated within the high crystallinity pluton generates the porphyry ore forming fluids. This scenario represents events within pluton underlying the IZP after emplacement of Tonalite 3 and between the intrusion of the Porphyritic Tonalite and the Chikora Tonalite Porphyry; E) Generation of zircon textures corresponding to the stages of the pluton's thermal evolution (A–D) (i) sector zoned, equant zircons evolve in a high crystallinity environment, (ii) resorption occurring during melt remobilisation and (iii) discordant rims and prismatic zircons grow following ascent and emplacement of the remobilised magma.

7. Conclusions

High precision U–Pb geochronology of the IZP demonstrates that multiple, nested and discrete ore forming magmatic hydrothermal events can occur within < ca. 50 kyr succession, and rapidly after major non-mineralising magmatic intrusions from the same plutonic source. Texturally, chemically and temporally characterised zircon supports that antecrystic crystals were recycled from a deeper silicic pluton accumulated over the 10^5 yr lifetime of the system. These precursor magmas were stored within a highly crystalline, H_2O saturated, immobile state. Geochronology and zircon dissolution rates constrain the durations that mobile porphyritic melt batches were available to be emplaced at shallower levels and transport PCD components to only a few thousand years. Porphyritic melts resulted from thermal perturbations of the high-crystallinity silicic magma, likely due to the percolation of hot S- ± metal-rich volatiles exsolved from contemporaneous, underlying andesitic magma. An intrinsic link between the generation of ore fluids and the extraction of the mobile, porphyritic melts from a high-crystallinity source pluton is implied. We attribute extensive mass transfer during magma mixing to the generation of the non-mineralising precursor apophyses of the pluton. The appropriate thermal conditions for ore formation are therefore ultimately controlled by magma flux rates to long-lived hydrous silicic plutons.

Acknowledgements

We thank Newmont Mining and SolGold for access and logistical support. Fieldwork was also facilitated by the Solomon Island Geological Survey. Work was funded by UoL and BGS University Funding Initiative PhD studentship (S176), NIGFSC (IP-1212-1110), and Society for Economic Geologists Newmont Student Research grant (2274). This manuscript was improved by comments of D. Sahy, two anonymous reviews and the thoughtful editorial handling of M. Bickle. This manuscript is published with the permission of the Executive Director, British Geological Survey (NERC).

Appendix A. Supplementary material

Supplementary material related to this article can be found online at http://dx.doi.org/10.1016/j.epsl.2016.02.046.

References

Bachmann, O., Bergantz, G.W., 2004. On the origin of crystal-poor rhyolites: extracted from batholithic crystal mushes. J. Petrol. 45, 1565–1582. http://dx.doi.org/10.1093/petrology/egh019.

Bachmann, O., Bergantz, G.W., 2006. Gas percolation in upper-crustal silicic crystal mushes as a mechanism for upward heat advection and rejuvenation of near-solidus magma bodies. J. Volcanol. Geotherm. Res. 149, 85–102. http://dx.doi.org/10.1016/j.jvolgeores.2005.06.002.

Barboni, M., Schoene, B., 2014. Short eruption window revealed by absolute crystal growth rates in a granitic magma. Nat. Geosci. 7, 524–528. http://dx.doi.org/10.1038/ngeo2185.

Blundy, J., Mavrogenes, J., Tattitch, B., Sparks, S., Gilmer, A., 2015. Generation of porphyry copper deposits by gas–brine reaction in volcanic arcs. Nat. Geosci. 8, 235–240. http://dx.doi.org/10.1038/ngeo2351.

Boehnke, P., Watson, B.E., Trail, D., Harrison, M.T., Schmitt, A.K., 2013. Zircon saturation re-revisited. Chem. Geol. 351, 324–334. http://dx.doi.org/10.1016/j.chemgeo.2013.05.028.

Burnham, C.W., 1997. Magmas and hydrothermal fluids. In: Barnes, H.L. (Ed.), Geochemistry of Hydrothermal Ore Deposits, 3rd edn. John Wiley & Sons, New York, pp. 63–123.

Candela, P.A., Holland, H.D., 1986. A mass transfer model for copper and molybdenum in magmatic hydrothermal systems, the origin of porphyry-type ore deposits. Econ. Geol. 81, 1–19. http://dx.doi.org/10.2113/gsecongeo.81.1.1.

Chivas, A.R., 1978. Porphyry copper mineralization at the Koloula igneous complex, Guadalcanal, Solomon Islands. Econ. Geol. 73, 645–677. http://dx.doi.org/10.2113/gsecongeo.73.5.645.

Chivas, A.R., Andrew, A.S., Sinha, A.K., O'Neil, J.R., 1982. Geochemistry of a Pliocene–Pleistocene oceanic-arc plutonic complex, Guadalcanal. Nature 300, 139–143. http://dx.doi.org/10.1038/300139a0.

Chivas, A.R., McDougall, I., 1978. Geochronology of the Koloula porphyry copper prospect, Guadalcanal, Solomon Islands. Econ. Geol. 73, 678–689. http://dx.doi.org/10.2113/gsecongeo.73.5.678.

Chivas, A.R., O'Neil, J.R., Katchan, G., 1984. Uplift and submarine formation of some Melanesian porphyry copper deposits: stable isotope evidence. Earth Planet. Sci. Lett. 68, 326–334. http://dx.doi.org/10.1016/0012-821x(84)90163-8.

Chivas, A.R., Wilkins, R.W.T., 1977. Fluid inclusion studies in relation to hydrothermal alteration and mineralization at the Koloula porphyry copper prospect, Guadalcanal. Econ. Geol. 72, 153–169. http://dx.doi.org/10.2113/gsecongeo.72.2.153.

Cooper, K.M., Kent, A.J.R., 2014. Rapid remobilization of magmatic crystals kept in cold storage. Nature 506, 480–483. http://dx.doi.org/10.1038/nature12991.

Corfu, F., 2003. Atlas of zircon textures. Rev. Mineral. Geochem. 53, 469–500. http://dx.doi.org/10.2113/0530469.

Couch, S., Sparks, R.S.J., Carroll, M.R., 2001. Mineral disequilibrium in lavas explained by convective self-mixing in open magma chambers. Nature 411, 1037–1039. http://dx.doi.org/10.1038/35082540.

Dilles, J.H., Kent, A.J.R., Wooden, J.L., Tosdal, R.M., Koleszar, A., Lee, R.G., Farmer, L.P., 2015. Zircon compositional evidence for sulfur-degassing from ore-forming arc magmas. Econ. Geol. 110, 241–251. http://dx.doi.org/10.2113/econgeo.110.1.241.

Ferry, J.M., Watson, E.B., 2007. New thermodynamic models and revised calibrations for the Ti-in-zircon and Zr-in-rutile thermometers. Contrib. Mineral. Petrol. 154, 429–437. http://dx.doi.org/10.1007/s00410-007-0201-0.

Gualda, G.A.R., Ghiorso, M.S., Lemons, R.V., Carley, T.L., 2012. Rhyolite-MELTS: a modified calibration of MELTS optimized for silica-rich, fluid-bearing magmatic systems. J. Petrol. 53, 875–890. http://dx.doi.org/10.1093/petrology/egr080.

Halter, W.E., Heinrich, C.A., Pettke, T., 2005. Magma evolution and the formation of porphyry Cu–Au ore fluids: evidence from silicate and sulfide melt inclusions. Miner. Depos. 39, 845–863. http://dx.doi.org/10.1007/s00126-004-0457-5.

Harris, A.C., Kamenetsky, V.S., White, N.C., Steele, D.A., 2004. Volatile phase separation in silicic magmas at Bajo de la Alumbrera Porphyry Cu–Au deposit, NW Argentina. Res. Geol. 54, 341–356. http://dx.doi.org/10.1111/j.1751-3928.2004.tb00210.x.

Harrison, M.T., Watson, B.E., Aikman, A.B., 2007. Temperature spectra of zircon crystallization in plutonic rocks. Geology 35. http://dx.doi.org/10.1130/g23505a.1.

Hattori, K.H., Keith, J.D., 2001. Contribution of mafic melt to porphyry copper mineralization: evidence from Mount Pinatubo, Philippines, and Bingham Canyon, Utah, USA. Miner. Depos. 36, 799–806. http://dx.doi.org/10.1007/s001260100209.

Hayden, L.A., Watson, B.E., 2007. Rutile saturation in hydrous siliceous melts and its bearing on Ti-thermometry of quartz and zircon. Earth Planet. Sci. Lett. 258, 561–568. http://dx.doi.org/10.1016/j.epsl.2007.04.020.

Hoskin, P.W.O., 2000. Patterns of chaos: fractal statistics and the oscillatory chemistry of zircon. Geochim. Cosmochim. Acta 64, 1905–1923. http://dx.doi.org/10.1016/s0016-7037(00)00330-6.

Huber, C., Bachmann, O., Manga, M., 2010. Two competing effects of volatiles on heat transfer in crystal-rich magmas: thermal insulation vs defrosting. J. Petrol. 51, 847–867. http://dx.doi.org/10.1093/petrology/egq003.

Huber, C., Bachmann, O., Vigneresse, J.-L., Dufek, J., Parmigiani, A., 2012. A physical model for metal extraction and transport in shallow magmatic systems. Geochem. Geophys. Geosyst. 13. http://dx.doi.org/10.1029/2012gc004042.

Ickert, R.B., Mundil, R., Magee, C.W., Mulcahy, S.R., 2015. The U–Th–Pb systematics of zircon from the Bishop Tuff: a case study in challenges to high-precision Pb/U geochronology at the millennial scale. Geochim. Cosmochim. Acta. http://dx.doi.org/10.1016/j.gca.2015.07.018.

Kaczmarek, M.-A., Reddy, S.M., Timms, N.E., 2011. Evolution of zircon deformation mechanisms in a shear zone (Lanzo massif, Western-Alps). Lithos 127, 414–426. http://dx.doi.org/10.1016/j.lithos.2011.09.016.

Kirkland, C.L., Smithies, R.H., Taylor, R.J.M., Evans, N., McDonald, B., 2015. Zircon Th/U ratios in magmatic environs. Lithos 212–215, 397–414. http://dx.doi.org/10.1016/j.lithos.2014.11.021.

Lake, E.T., 2013. Crystallization and saturation front propagation in silicic magma chambers. Earth Planet. Sci. Lett. 383, 182–193. http://dx.doi.org/10.1016/j.epsl.2013.09.039.

Leuthold, J., Müntener, O., Baumgartner, L.P., Putlitz, B., Ovtcharova, M., Schaltegger, U., 2012. Time resolved construction of a bimodal laccolith (Torres del Paine, Patagonia). Earth Planet. Sci. Lett. 325–326, 85–92. http://dx.doi.org/10.1016/j.epsl.2012.01.032.

Marsh, B.D., 1981. On the crystallinity, probability of occurrence, and rheology of lava and magma. Contrib. Mineral. Petrol. 78, 85–98. http://dx.doi.org/10.1007/BF00371146.

Menand, T., Annen, C., de Saint Blanquat, M., 2015. Rates of magma transfer in the crust: insights into magma reservoir recharge and pluton growth. Geology 43, 199–202. http://dx.doi.org/10.1130/g36224.1.

Miller, J.S., Matzel, J.E.P., Miller, C.F., Burgess, S.D., Miller, R.B., 2007. Zircon growth and recycling during the assembly of large, composite arc plutons. J. Volcanol. Geotherm. Res. 167, 282–299. http://dx.doi.org/10.1016/j.jvolgeores.2007.04.019.

Mungall, J.E., Brenan, J.M., Godel, B., Barnes, S.J., Gaillard, F., 2015. Transport of metals and sulphur in magmas by flotation of sulphide melt on vapour bubbles. Nat. Geosci. 8, 216–219. http://dx.doi.org/10.1038/ngeo2373.

Nadeau, O., Stix, J., Williams-Jones, A.E., 2013a. The behavior of Cu, Zn and Pb during magmatic–hydrothermal activity at Merapi volcano, Indonesia. Chem. Geol. 342, 167–179. http://dx.doi.org/10.1016/j.chemgeo.2013.01.018.

Nadeau, O., Williams-Jones, A.E., Stix, J., 2013b. Magmatic–hydrothermal evolution and devolatilization beneath Merapi volcano, Indonesia. J. Volcanol. Geotherm. Res. 261, 50–68. http://dx.doi.org/10.1016/j.jvolgeores.2013.04.006.

Parmigiani, A., Huber, C., Bachmann, O., 2014. Mush microphysics and the reactivation of crystal-rich magma reservoirs. J. Geophys. Res., Solid Earth 119, 6308–6322. http://dx.doi.org/10.1002/2014jb011124.

Pasteris, J.D., 1996. Mount Pinatubo volcano and 'negative' porphyry copper deposits. Geology 24. http://dx.doi.org/10.1130/0091-7613(1996)024<1075:mpvanp>2.3.co;2.

Petterson, M., Babbs, T., Neal, C., Mahoney, J., Saunders, A., Duncan, R., Tolia, D., Magu, R., Qopoto, C., Mahoa, H., Natogga, D., 1999. Geological–tectonic framework of Solomon Islands, SW Pacific: crustal accretion and growth within an intra-oceanic setting. Tectonophysics 301, 35–60. http://dx.doi.org/10.1016/s0040-1951(98)00214-5.

Pistone, M., Caricchi, L., Ulmer, P., Reusser, E., Ardia, P., 2013. Rheology of volatile-bearing crystal mushes: mobilization vs. viscous death. Chem. Geol. 345, 16–39. http://dx.doi.org/10.1016/j.chemgeo.2013.02.007.

Von Quadt, A., Erni, M., Martinek, K., Moll, M., Peytcheva, I., Heinrich, C.A., 2011. Zircon crystallization and the lifetimes of ore-forming magmatic–hydrothermal systems. Geology 39, 731–734. http://dx.doi.org/10.1130/g31966.1.

Reddy, S.M., Timms, N.E., Kinny, P.D., 2006. Geochemical modification of plastically deformed zircon. Geochim. Cosmochim. Acta 70. http://dx.doi.org/10.1016/j.gca.2006.06.961.

Richards, J.P., 2011. High Sr/Y arc magmas and porphyry Cu Mo Au deposits: just add water. Econ. Geol. 106, 1075–1081. http://dx.doi.org/10.2113/econgeo.106.7.1075.

Rivera, T.A., Storey, M., Schmitz, M.D., Crowley, J.L., 2013. Age intercalibration of $^{40}Ar/^{39}Ar$ sanidine and chemically distinct U/Pb zircon populations from the Alder Creek Rhyolite Quaternary geochronology standard. Chem. Geol. 345, 87–98. http://dx.doi.org/10.1016/j.chemgeo.2013.02.021.

Schoene, B., Schaltegger, U., Brack, P., Latkoczy, C., Stracke, A., Günther, D., 2012. Rates of magma differentiation and emplacement in a ballooning pluton recorded by U–Pb TIMS-TEA, Adamello batholith, Italy. Earth Planet. Sci. Lett. 355–356, 162–173. http://dx.doi.org/10.1016/j.epsl.2012.08.019.

Schärer, U., 1984. The effect of initial ^{230}Th disequilibrium on young U–Pb ages: the Makalu case, Himalaya. Earth Planet. Sci. Lett. 67, 191–204. http://dx.doi.org/10.1016/0012-821x(84)90114-6.

Shinohara, H., Hedenquist, J.W., 1997. Constraints on magma degassing beneath the far southeast porphyry Cu–Au deposit, Philippines. J. Petrol. 38, 1741–1752. http://dx.doi.org/10.1093/petroj/38.12.1741.

Sillitoe, R.H., 2010. Porphyry copper systems. Econ. Geol. 105, 3–41. http://dx.doi.org/10.2113/gsecongeo.105.1.3.

Sparks, R.S.J., Marshall, L.A., 1986. Thermal and mechanical constraints on mixing between mafic and silicic magmas. J. Volcanol. Geotherm. Res. 29, 99–124. http://dx.doi.org/10.1016/0377-0273(86)90041-7.

Spera, F., 1980. Thermal evolution of plutons: a parameterized approach. Science 207, 299–301. http://dx.doi.org/10.1126/science.207.4428.299.

Swiridiuk, P., 1998. Exploring the Solomon Islands with airborne geophysics. Explor. Geophys. 29. http://dx.doi.org/10.1071/eg998620.

Vasyukova, O.V., Kamenetsky, V.S., Goemann, K., Davidson, P., 2013. Diversity of primary CL textures in quartz from porphyry environments: implication for origin of quartz eyes. Contrib. Mineral. Petrol. 166, 1253–1268. http://dx.doi.org/10.1007/s00410-013-0923-0.

Vavra, G., 1990. On the kinematics of zircon growth and its petrogenetic significance: a cathodoluminescence study. Contrib. Mineral. Petrol. 106, 90–99. http://dx.doi.org/10.1007/bf00306410.

Vermeesch, P., 2012. On the visualisation of detrital age distributions. Chem. Geol. 312–313, 190–194. http://dx.doi.org/10.1016/j.chemgeo.2012.04.021.

Wallace, P.J., Edmonds, M., 2011. The sulfur budget in magmas: evidence from melt inclusions, submarine glasses, and volcanic gas emissions. Rev. Mineral. Geochem. 73, 215–246. http://dx.doi.org/10.2138/rmg.2011.73.8.

Watson, B.E., 1996. Dissolution, growth and survival of zircons during crustal fusion: kinetic principles, geological models and implications for isotopic inheritance. In: Special Paper 315: The Third Hutton Symposium on the Origin of Granites and Related Rocks, pp. 43–56.

Watson, E.B., Liang, Y., 1995. A simple model for sector zoning in slowly grown crystals; implications for growth rate and lattice diffusion, with emphasis on accessory minerals in crustal rocks. Am. Mineral. 80, 1179–1187.

Wilkinson, J.J., 2013. Triggers for the formation of porphyry ore deposits in magmatic arcs. Nat. Geosci. 6, 917–925. http://dx.doi.org/10.1038/ngeo1940.

Zajacz, Z., Halter, W., 2009. Copper transport by high temperature, sulfur-rich magmatic vapor: evidence from silicate melt and vapor inclusions in a basaltic andesite from the Villarrica volcano (Chile). Earth Planet. Sci. Lett. 282, 115–121. http://dx.doi.org/10.1016/j.epsl.2009.03.006.